# Structural basis for antibody cross-neutralization of Dengue and Zika viruses

Nicholas K. Hurlburt[1], Jay Lubow[1], Leslie Goo,[1*] Marie Pancera[1]

[1]Vaccine and Infectious Disease Division, Fred Hutchinson Cancer Center, Seattle, Washington, USA.

*Current address: Vaccine Company, Inc., South San Francisco, California, USA

Correspondence: mpancera@fredhutch.org

**Abstract**

Safe and effective vaccines against co-circulating mosquito-borne orthoflaviviruses such as Zika virus (ZikV) and the four serotypes of Dengue virus (DenV1-4) must elicit broadly neutralizing antibodies (bnAbs) to prevent the risk of enhancement of infection by non-neutralizing antibodies. We recently discovered new orthoflavivirus-directed bnAbs, including F25.S02, which neutralizes DenV1-4 and ZikV with comparable or superior potency to the previously characterized E dimer epitope (EDE) bnAbs. Mutagenesis studies of viral envelope proteins showed that the epitope specificity of F25.S02 is distinct from EDE1 bnAbs. Here, we used cryoEM and X-ray crystallography to understand the basis of cross-neutralization of F25.S02 at the molecular level. We obtained a ~4.2 Å cryoEM structure of F25.S02 Fab bound to a stabilized DenV3 soluble E protein dimer and a 2.3 Å crystal structure of F25.S02 Fab bound to ZikV soluble E protein dimer. Like previously described EDE1 bnAbs, the structural epitope of F25.S02 is at the E dimer interface, encompassing predominantly conserved regions in domain II, including the fusion loop. However, unlike EDE1 bnAbs, F25.S02 binding is almost entirely dependent on the heavy chain and is shifted slightly away from the dimer symmetry axis. Our findings emphasize the importance of this cross-neutralizing site of vulnerability for DenV and ZikV that can facilitate rational design of vaccines and therapeutics.

25

26 **Introduction**

27 Orthoflaviviruses are arthropod-borne, enveloped RNA viruses that can cause symptoms ranging from a
28 self-limiting fever to potentially fatal hemorrhagic or neuroinvasive disease for which there is no
29 treatment beyond supportive care. Many orthoflaviviruses are emerging threats to global health: the four
30 DenV serotypes (DenV1-4) infect an estimated 390 million people annually[1]; ZikV emerged outside of
31 Asia and Africa for the first time in 2007 and was repeatedly introduced into the Americas in 2014-2015,
32 leading to considerable morbidity[2]. The ability of orthoflaviviruses to rapidly emerge from relative
33 obscurity to serious public health threats combined with the geographical expansion of mosquito
34 vectors[3], further facilitated by climate change [4], underscores the importance of effective clinical
35 interventions.

36 The envelope (E) protein of orthoflaviviruses, including DenV1-4 and ZikV, is a key structural protein
37 involved in viral entry and membrane fusion, and is the target of antibodies [5]. The soluble form of this
38 protein (sE) retains many of the antigenic properties of the native virion-associated E protein [6]. While
39 structurally conserved across DenV1–4 and ZikV, variations in sE can influence virus-specific interactions
40 with host antibodies and receptors, impacting cross-reactivity and immune protection [7].

41 The complex antibody response to co-circulating and antigenically related orthoflaviviruses presents a
42 major challenge for vaccine development. Specifically, the presence of cross-reactive, non-neutralizing
43 antibodies to E protein from a prior exposure to ZikV or a given DenV serotype predicts the risk of severe
44 disease following secondary exposure to a different DenV serotype[8, 9] - a process known as antibody-
45 dependent enhancement (ADE) of infection. To minimize the risk of ADE, a safe and effective vaccine must
46 elicit antibodies that simultaneously neutralize DenV1-4, and ideally, ZikV. Despite decades of research,
47 ADE-related safety concerns ultimately derailed the widespread use of the first licensed DenV vaccine[10].
48 This unfortunate outcome eroded public confidence in vaccines in general[11]. Thus, although many

49 successful vaccines have been developed without first knowing the specific targets of the antibodies they
50 elicited, such empirical approaches to developing DenV vaccines have been insufficient. A rational
51 approach to vaccine design to limit the elicitation of non-neutralizing antibodies is needed and this
52 requires improving our fundamental understanding of how orthoflavivirus bnAbs recognize their targets.
53 A few bnAbs that can potently neutralize DenV1-4 and in some cases, ZikV, have been isolated from
54 infected individuals. The most well-characterized bnAbs target an envelope-dimer epitope (EDE) spanning
55 both E protein protomers within the dimer subunit as defined by X-ray crystallography and cryo-electron
56 microscopy (cryo-EM)[12, 13]. There are two subclasses of EDE bnAbs, of which EDE1 but not EDE2 can
57 potently neutralize ZikV in addition to DenV1-4[14]. Until recently, SIgN-3C was the only known naturally
58 occurring, cross-neutralizing antibody outside the EDE1 class[15]. Unlike EDE antibodies, which target an
59 *intra*-dimer epitope, SIgN-3C binds an epitope at the *inter*-dimer interface[16], as determined by cryo-EM.
60 Recently, we identified F25.S02, another naturally occurring bnAb with broad and potent cross-
61 neutralization of DenV1-4 and ZikV [17]. Mutational and neutralization analysis showed that the F25.S02
62 epitope was distinct from the EDE1 bnAb C10 [17]. Here, we determined the binding mechanism of
63 F25.S02 to DenV3 sE dimer by cryoEM and to ZikV sE dimer using X-ray crystallography. The structures
64 revealed that F25.S02 differs in its mode of binding compared to other cross-neutralizing EDE1 antibodies.
65 Our results can ultimately guide structure-based vaccine design, the promise of which is best exemplified
66 by the recently approved vaccine for respiratory syncytial virus[18].
67

68 **Results**

69 **F25.S02 binds a highly conserved patch on DenV3 sE**

70 We previously showed that F25.S02 had the highest neutralization potency against DenV3[17]. We
71 expressed and purified a previously described stabilized sE protein dimers (DenV3 sE sc30)[19] and a His-
72 tagged antigen binding fragment (Fab) of F25.S02. We formed a stable complex as indicated by a

73 monodisperse peak by size-exclusion chromatography (SEC) (**Supplementary Fig. 1a**) and used this
74 complex to obtain a cryoEM reconstruction to 4.2 Å resolution (**Fig. 1a, Supplementary Fig. 2,**
75 **Supplementary Table 1**)**.** The map revealed the sE dimer with two Fabs bound at the envelope dimer
76 interface, similar to what has been shown with previously identified EDE1 antibodies [14, 20]. F25.S02
77 interacts with domain I and III of one protomer and domain II and fusion loop of the other protomer (**Fig.**
78 **1A**). The local resolution of the F25.S02 for most of the binding site is around 3.5 Å, increasing the
79 confidence in sidechain assignment (**Supplementary Fig. 2d, e**). F25.S02 binds DenV3 with a total buried
80 surface area (BSA) of ~1,157 $Å^2$ with ~1,010 $Å^2$ from the heavy chain (HC) and ~147 $Å^2$ from the light chain
81 (LC). Thus, nearly 87% of the BSA comes from the HC (**Fig. 1B**). The F25.S02 binding site is a highly
82 conserved patch on the E protein among all DenV serotypes and ZikV (**Fig. 1C**) as shown by mapping the
83 surface with a conservation score generated by the Consurf server[21].
84 The cryoEM map shows clear density for the first N-acetylglucosamine (GlcNAc) of the N67 glycan
85 (**Supplementary Fig. 3a**) and two GlcNAc and one mannose of the N153 glycan (**Supplementary Fig. 3b**);
86 both glycans are conserved among DenV serotypes. F25.S02 does not contact the glycan at N67 but
87 interacts with the glycan at N153. This was unexpected because we previously showed that mutations at
88 either N153 or T155 to remove the glycan increased F25.S02 neutralization potency against DenV2 [17].
89 To determine if the glycan was needed for DenV3 recognition, we removed the glycan by mutating
90 threonine 155 to alanine (T155A) and tested binding of F25.S02 to DenV3 sE sc30 T155A by biolayer
91 interferometry (BLI). The BLI data showed that the T155A mutation had no effect on F25.S02 Fab binding
92 to DenV3 sE sc30, indicating that the N153 glycan is not necessary for binding (**Supplementary Fig. 1b**)
93 even though it contributes ~213 $Å^2$ of buried surface area (18% of the total BSA for DenV3).
94
95 **F25.S02 binds ZikV sE at the E dimer interface**

96 As F25.S02 cross-neutralized DenV and ZikV, we next determined its structure bound to ZikV to
97 understand the basis of its cross-reactivity. The wildtype (WT) ZikV sE dimer showed high affinity binding
98 for F25.S02 (**Supplementary Fig. 1c**). To increase yield for structural studies, we co-expressed ZikV sE WT
99 with F25.S02 Fab and obtained enough complex for crystallization experiments. The purified complex was
100 confirmed by SEC to be sE dimer with two Fabs bound (**Supplementary Fig. 1d**). Well diffracting crystals
101 were obtained, and an X-ray structure was determined to 2.3 Å resolution (**Fig. 2a, Supplementary Table**
102 **2**). The crystal had a $P4_12_12$ space group with an sE dimer and two Fabs in the asymmetric unit (ASU). The
103 structure was solved by molecular replacement with $R_{work}$ and $R_{free}$ of 0.225 and 0.274, respectively
104 (**Supplementary Table 2**). Like in the DenV3 structure, the ZikV structure shows that the F25.S02 epitope
105 is mostly HC dependent, accounting for ~77% of the total BSA (**Fig2. b, f**). The total BSA of F25.S02 on ZikV
106 is ~1,464 $Å^2$ with ~1,130 $Å^2$ from the HC and ~334 $Å^2$ from the LC. All three CDRHs are involved in binding
107 but only the CDRL2 is involved in binding with single residues in framework region (FR) 2 and FR3 having
108 minor contributions (**Fig. 2f**).
109 The majority of the interactions between F25.S02 and ZikV sE are located on domain II and the fusion loop
110 of protomer A (**Fig. 2c**). The CDRH2 sits in a shallow pocket formed by the fusion loop, the β-strand *b* and
111 the *ij* loop of domain II. The CDRH3 contains a one turn α-helix and sits on the surface formed by β-strand
112 *b* and the fusion loop. $Glu_{73HC}$ in FR3 of the HC forms a H-bond with $Arg_{252ZikV}$ in domain II while $Ser_{74HC}$ of
113 FR3 interacts with $Asp_{278ZikV}$ of protomer B. The CDRH1 of F25.S02 interacts with the 150 loop of domain I
114 of protomer B, which contains the N154 glycan (**Fig. 2d**), that is equivalent to N153 in DenV (of note, ZikV
115 lacks the glycan at position 67 present in DenV). Interactions between F25.S02 LC and ZikV sE are all
116 located on domain III with the CDRL2 forming three H-bonds with domain III of protomer B. The HC forms
117 a single interaction with domain III with $Leu_{100EHC}$ sitting between $Lys_{316}$ of one protomer and the fusion
118 loop of the other (**Fig. 2e**).

119 The N154 glycan is well resolved in the electron density, unlike in many other structures of antibodies
120 bound to orthoflavivirus sE proteins [14, 20]. For both protomers, electron density can clearly be seen up
121 to the branching mannose, with electron density resolving the α1-3 and α1-6 mannose in protomer A
122 while only the α1-3 mannose is seen with protomer B (**Fig. 2d, Supplementary Fig. 3c, d**). Interestingly,
123 there are numerous interactions and H-bonds between F25.S02 and the N154 glycan. The first two N-
124 terminal residues of the HC interact with the first and second GlcNAc and $Arg_{94HC}$ forms a hydrogen bond
125 with the C3 hydroxyl of the first GlcNAc. Additionally, $Lys_{42LC}$ and $Lys_{45LC}$ of the LC interact with α1-3
126 mannose with $Lys_{45LC}$ forming a H-bond with the C4 hydroxyl (**Fig. 2d**). In total, the interactions with the
127 N154 glycan account for ~23% of the total BSA (350 $Å^2$) between F25.S02 and ZikV sE (**Fig. 2f**). Due to poor
128 expression levels of ZikV sE WT, we were not able to produce enough to confirm if the removal of the
129 glycan would affect F25.S02 binding affinity but it was previously shown that removal of the N154 glycan
130 increased the neutralization potency of F25.S02 against ZikV [22], indicating that the glycan is not required
131 for binding or neutralization.
132
133 **F25.S02 binds ZikV sE in a nearly identical manner as DenV3**
134 The residues of F25.S02 that interact with ZikV sE and DenV3 sE dimers are highly similar and most V-gene
135 interactions are germline encoded, with only $Met_{51HC}$ being mutated from Ile (**Fig. 2f**). An alignment of the
136 sE dimer of the ZikV and DenV3-F25.S02 bound structures shows good overlap with a root mean square
137 deviation (RMSD) of 3.94 Å over 775 paired α carbons (Cα) (**Fig. 3a**). DenV3-bound F25.S02 Fv is shifted
138 outward slightly relative to the ZikV-bound F25.S02 Fv, but this is mostly due to the slight difference in
139 conformations of the sE proteins. When aligning the Fv domains of one of the F25.S02 Fabs in each
140 structure, the overall RMSD is 1.02 Å over 234 paired Cα (**Fig. 3b**). In this alignment, the fusion loop and
141 bound portions of domain II almost completely overlap. If you remove the interactions with the
142 N153/N154 glycan from the BSA data, F25.S01 binds DenV3 sE with 85% HC and ZikV sE with 82% HC. The

143 contact with the glycan in ZikV is 222 $Å^2$ from the HC and 128 $Å^2$ from the LC, while in DenV3, the HC and
144 LC contact with an area of 201 and 13 $Å^2$, respectively. The LC binding contribution to the glycans in the
145 ZikV bound structure explains the difference between the 87% vs 77% overall BSA contribution of the HC
146 to Denv3 versus ZikV. In all, F25.S02 primarily utilizes its HC to bind to the highly conserved fusion loop of
147 DenV1-4 and ZikV. The light chain interactions are primarily with main chain atoms of ZikV sE that are not
148 highly conserved, the only side chain H-bond is from $Arg_{54LC}$ to $Glu_{370ZikV}$ in ZikV and a similar residue ($Glu_{370}$
149 in DenV1 and 3, $Asp_{370}$ in DenV2 and Asn in DenV4) is present in DenV1-4 that would be capable of forming
150 this interaction (**Fig. 3c**).
151
152 **F25.S02 binds a similar but distinct epitope to EDE1 antibodies**
153 We compared the binding mechanism of F25.S02 to two EDE1 bnAbs, C8[14] and C10[20], which also
154 cross-neutralize DenV1-4 and ZikV. An alignment of the ZikV-bound C8 and C10 to ZikV-bound F25.S02
155 structure shows that both C8 and C10 have a larger footprint on domain II and bind closer to the dimer
156 symmetry axis (**Fig. 4a**). Both C8 and C10 were shown to interact with N67 glycan on DenV (absent in ZikV)
157 that is not required for binding or neutralization [14, 20]. F25.S02 does not interact with this glycan on
158 DenV3 (**Fig. 3b**). For both C8 and C10, the CDRL3 occupies the position of the F25.S02 CDRH3 (**Fig. 4b**),
159 highlighting this shift towards the center of the sE dimer. An alignment of the Fv domains of C8 and C10
160 to F25.S02 further shows the distinction between the binding mechanisms. When C8 is aligned with
161 F25.S02, the two Fv domains align with an RMSD of 2.73 Å over 227 paired Cα. The C8-bound sE dimer is
162 shifted toward the interior relative to the F25.S02-bound sE dimer (**Fig. 4c, top**). When C10 is aligned with
163 F25.S02, the Fv domains have an RMSD of 2.50 Å over 233 paired Cα. Not only is the sE dimer shifted to
164 the center relative to F25.S02 bound ZikV sE, but the angle of approach is rotated about 20° (**Fig. 4c,**
165 **bottom**). In comparison, C8 and C10 have an RMSD of 2.01 Å over 229 paired Cα, highlighting that F25.S02
166 is more distinct from C8 and C10 than they are from each other. The difference in binding is further shown

167 by comparing the footprint on the ZikV sE dimer (**Fig. 4d**). Both C8 and C10 bind with a nearly equal split
168 of BSA between HC and LC. C8 has a HC contribution of 46% and C10 has a HC contribution of 50% to ZikV
169 sE, while F25.S02 is 82% HC binding by BSA (**Fig. 4f**).
170 Another cross-neutralizing bnAb against DenV1-4 and ZikV is SIgN-3C, which differs from EDE1 antibodies
171 by making both intra- and inter-dimer contacts [16]. When compared to F25.S02, SIgN-3C binding
172 footprint on ZikV sE is shifted away from domain I of the intra-dimer pair and to the exterior face of the
173 adjacent dimer, interacting with both domain I and II (**Fig. 4e**). SIgN-3C binds with a similar amount of BSA
174 as F25.S02 and is also mostly HC dependent (**Fig. 4f**), but its footprint is shifted to make the inter-dimer
175 interaction (**Fig. 4d, bottom**). In all, F25.S02 binds a similar epitope as EDE1 antibodies but employs a
176 distinct method of binding that is HC dependent and is confined to intra-dimer interactions, unlike SIgN-
177 3C.
178
179 **Discussion**
180 Our structural analysis of F25.S02, a potent cross-neutralizing antibody against ZikV and the four DenV
181 serotypes, reveals a common heavy chain-dominant binding mechanism to a highly conserved patch on
182 the E protein at the interface of the two protomers. The F25.S02 epitope encompasses domain II and the
183 fusion loop of one protomer and domains I and III of the other protomer in the sE dimer. Interestingly, it
184 appears that F25.S02 can readily accommodate glycans within the epitope but is not glycan-dependent
185 for binding or neutralization. This has been observed in HIV envelope-directed antibodies where bnAbs
186 mature to accommodate glycans but are not needed for neutralization [23-25].
187
188 The main differences in binding of F25.S02 to DenV3 and ZikV are observed at the residue insertion
189 present in ZikV. First, the insertion in the domain I loop, which includes the glycan at position N153/N154
190 (DenV3/ZikV, respectively), results in $N154_{ZikV}$ being in closer proximity to the F25.S02 Fab, with its light

191 chain making additional glycan contacts as seen in that structure (**Fig. 2d and Supplementary Fig. 3**).
192 Second, the insertion in domain III (residues 359-360 in DenV3, residues 370-373 in ZikV) also contributes
193 to more interactions of ZikV sE with F25.S02 light chain compared to DenV3 (**Fig. 2e**).

194 The analysis suggests F25.S02 crosslinks the dimer, which would inhibit conformational changes required
195 for viral fusion with the host membrane. This mechanism of neutralization has been reported for EDE1
196 bnAbs, which also cross-neutralize DenV1-4 and ZikV [14, 20]. However, as we only obtained structures
197 with the sE dimer, we cannot conclude if F25.S02 would induce a similar conformational change as EDE1
198 antibodies on viral particles [17]. We presently do not observe the asymmetric conformation reported
199 before of the sE dimer and thus cannot readily explain the differences in affinity and potency observed
200 for F25.S02 with ZikV and DenV1-4 [20]. In addition, we did not obtain structures of F25.S02 with the other
201 DenV serotypes and could not come up with a plausible explanation for the reported differences in
202 neutralization potency across serotypes by modeling the interactions at the residue level [20].

203 Further structural studies with the virions would need to be done to determine how F25.S02 binds to E
204 protein in its native form on the viral particle. We nevertheless modeled F25.S02 Fab binding to the virus,
205 by aligning our F25.S02-ZikV sE crystal structure on the whole virus cryoEM structure of ZikV (PDBid 6CO8)
206 [26] (**Fig. 5a**). The alignment indicated F25.S02 Fab could bind on the particle in every position on the
207 three-dimer raft (**Fig. 5c**), as well as all positions around the 3-fold symmetry axis (**Fig. 5b**) without steric
208 clashes. There could be a potential clash of F25.S02 light chain at the 5-fold symmetry axis (5f position)
209 (**Fig. 5d**) that could have an impact on the avidity of binding of F25.S02 antibody as seen for other EDE1
210 antibodies [20].
211

212 While F25.S02's epitope is similar to previously reported cross-neutralizing EDE-antibodies, its binding
213 mode is distinct as 1) it uses predominantly heavy chain recognition, 2) its binding is shifted away from

214 the 2-fold symmetry axis of the dimer and N67 glycan in DenV3, and 3) most of its interactions are
215 mediated by germline residues [14, 20]. With SIgN-3C and F25.S02, the interactions to ZikV E protein use
216 a similar footprint area and both utilize a predominantly heavy chain mode of binding, but F25.S02 lacks
217 the inter-dimer interactions that are necessary for SIgN-3C recognition [16]. Thus, F25.S02 binds a similar
218 site with a distinct mode of binding and could be a distinct class of cross-neutralizing antibody.
219
220 The structural information that F25.S02 binds a highly conserved epitope present on both ZikV and DenV,
221 and that its mode of binding is primarily heavy chain dependent with little affinity maturation required
222 for broad neutralization makes its epitope an interesting target for rational or computational vaccine
223 design that would elicit broadly neutralizing antibodies.
224
225
226
227
228
229
230
231
232
233
234
235
236
237

238

239

240

241 **Methods**

242 **Fab expression and purification**

243 The gene encoding the variable region of the heavy chain of F25.S02 was cloned into a vector with a
244 human CH1 domain with a C-terminal his-tag using the Platinum SuperFi II DNA polymerase
245 (ThermoFisher, 12368010) and the In-Fusion cloning system (Takara Bio, 638948). The Fab was expressed
246 in HEK293E (RRID:CVCL_HF20) cells at $1\times10^6$ cells/mL using a total of 500 µg DNA per liter of culture (1:1
247 ratio of HC-to-LC DNA). PEI was used as the transfection reagent at a ratio of 4:1 PEI-to-DNA. Culture was
248 harvested after 6 days and Fab was purified from cultural supernatant using His60 Ni Superflow resin
249 (Takara Bio). Fab was eluted from column using buffer containing 50 mM Tris, pH 7.5, 300 mM NaCl, and
250 150 mM Imidazole. F25.S02 Fab was further purified using a HiLoad 16/600 Superdex 200 size exclusion
251 column (Cytivia) on an AKTApure system (GE Biosciences) into a buffer containing 5 mM HEPES, 150 mM
252 NaCl, pH 7.5.

253

254 **sE protein expression**

255 Plasmids for WT and stabilized sE proteins were kindly provided by Brian Kulhman (University of North
256 Carolina at Chapel Hill) [19]. sE proteins were expressed in Expi293F cells according to manufacturer's
257 protocol (ThermoFisher, A14635). Cultures were harvested 6 days after transfection and cleared
258 supernatant was incubated with His60 Ni Superflow resin (Takara Bio, 635660). sE protein was eluted from
259 column using buffer containing 50 mM Tris, pH 7.5, 300 mM NaCl, and 300 mM imidazole. For structural
260 studies, protein was further purified by size exclusion chromatography (SEC) using a HiLoad 16/600
261 Superdex 200 column (Cytiva) or a Superdex 200 Increase 10/300 column (Cytiva) on a AKTApure system

262 (GE Biosciences). SEC peak corresponding to dimer was kept and concentrated using a 10K MWCO Amicon
263 Ultra Centrifugal Filter (Millipore Sigma, UFC901024).
264 Plasmid for DenV3 sE sc30 T155A was made via site-directed mutagenesis using the Platinum SuperFi II
265 DNA polymerase (ThermoFisher, 12368010) and DenV3 sE sc30 T155A expressed and purified as above.
266
267 **sE+F25.S02 complex formation**
268 For DenV3 sE sc30, sE protein was mixed with F25.S02 Fab in a 1:2.5 dimer-to-Fab ratio for 2 hours at 4°C
269 with nutation. Complex was purified on a HiLoad 16/600 Superdex 200 column (Cytiva) and fractions
270 corresponding to complex were pooled and concentrated to $OD_{280}$=8. Complex was divided into 20 µL
271 aliquots, flash frozen in LN2, and stored at -80°C.
272 For the ZikV sE WT + F25.S02 Fab complex, the plasmid for ZikV sE WT was mutated to remove the 8x His-
273 tag using the In-Fusion cloning system (Takara Bio, 638948). Complex was expressed in Expi293F cells
274 according to manufacturer's protocol using a plasmid DNA ratio of 2:1:1 sE-to-HC-to-LC. Culture was
275 harvested 6 days after transfection and complex was purified from cultural supernatant using His60 Ni
276 Superflow resin (Takara Bio). Protein was eluted using buffer containing 50 mM Tris, pH 7.5, 300 mM NaCl,
277 and 300 mM Imidazole. Complex was further purified using a HiLoad 16/600 Superdex 200 size exclusion
278 column (Cytivia) on an AKTApure system (GE Biosciences) into a buffer containing 5 mM HEPES, 150 mM
279 NaCl, pH 7.5. Fractions corresponding to complex were pooled and concentrated to $OD_{280}$=25, divided into
280 50 µL aliquots and flash frozen in LN2. All aliquots were stored at -80°C.
281
282 **Biolayer interferometry**
283 F25.S02 binding was measured using biolayer interferometry on an Octet 96 Red instrument (ForteBio)
284 using FAB2G biosensors (Sartorius). F25.S02 Fab was diluted to 10 µg/mL in kinetics buffer (1× PBS, 0.01%
285 Tween 20, 0.01% BSA and 0.005% NaN3, pH 7.4). Each sE protein was diluted to 1 µM in kinetics buffer.

286 Fab was loaded onto biosensor until a threshold of 1.0 nm shift was reached. After loading, biosensors
287 were placed in kinetics buffer for 60 sec for a baseline reading. Biosensors were then immersed in analyte
288 for 300 sec in the association phase, followed by 300 sec in the dissociation phase in kinetics buffer. The
289 background signal from a biosensor loaded with Fab but with no analyte was subtracted from each loaded
290 biosensor.
291
292 **CryoEM sample preparation**
293 DenV3 sE sc30+F25.S02 Fab complex was thawed and diluted to $OD_{280}$=5. Just prior to grid preparation,
294 complex was mixed with 0.1% Tween20 to a final concentration of 0.25 CMC (0.5 µL of 0.1% Tween20 into
295 20 µL of complex). 3 µL of complex was loaded onto UltrAuFoil R1.2/1.3 300mesh grids (Ted Pella) and
296 manually blotted. Another 3 µL was loaded onto grid and vitrified on a Vitrobot Mark IV (ThermoFisher)
297 with a blot force of 2, blot time of 4 sec at 4°C and 100% humidity before plunging into liquid ethane.
298
299 **CryoEM data collection and processing**
300 Data was collected on a 200 kV Glacios microscope (ThermoFisher) with a K3 direct electron detector
301 (Gatan) at a magnification of 36,000x (1.122 Å per pixel) using SerialEM [27]. A total of 1,195 movies were
302 collected with 100 exposures over 6 sec. Motion correction was performed using Warp [28] and processed
303 using cryoSPARC (V4.5) [29]. Initial 2D templates were generated through multiple rounds of 2D
304 classification. Using 2D templates, particles were re-extracted using template picker. A total of ~2 million
305 particles were extracted and after 3 rounds of 2D classification, 111,111 particles were used for Ab-initio
306 reconstruction without symmetry. The reconstruction was refined using homogenous refinement
307 followed by non-uniform refinement [30] with C2 symmetry. Local refinement was performed using a
308 mask to exclude the Fc domain of F25.S02. The FSC curve suggested heterogeneity in the particles and a
309 3D classification was used to separate particles into two classes. Following homogeneous refinement, one

310 class showed better quality and was further refined with local refinement with a mask to exclude the Fc
311 domain and 64,110 particles. The resolution was estimated to be 4.16 Å per the gold standard $FSC_{0.143}$.
312 Local resolution was estimated based on gold standard $FSC_{0.143}$ and is shown in **Supplementary Fig. 2**.
313

314 **CryoEM model building and refinement**

315 The model of DenV3 sE protomer from PDBid 7A3P [20] was used as the initial model and a model of
316 F25.S02 Fab was generated by AlphaFold3 [31]. Both models were docked into the cryoEM map using
317 ChimeraX (v1.9) [32]. Model building was completed using Coot (v0.9.8.1) [33] and an initial refinement
318 was run using Phenix (v1.21) real_space_refinement [34]. Further refinement was performed using
319 ISOLDE [35] in ChimeraX [32] and Coot [33]. Data collection and refinement statistics are summarized in
320 **Supplementary Table 1**. Structural figures were generated using ChimeraX and the conserved residue
321 map was generated using the ConSurf web server [21] with the E protein sequences from the reference
322 strains of DenV1-4 and ZikV. BSA data was determined using the PDBePISA server [36].
323

324 **Crystallization and structure determination**

325 Initial crystallization screening was performed by sitting-drop vapor diffusion using ProPlex crystallization
326 screen (Molecular Dimensions) and an NT8 drop setting robot (Formulatrix) at a complex concentration
327 of $OD_{280}$=15. Initial crystals grew in drop F5 (0.1 M Tris, pH 8.0, 0.1 M NaCl, 8% w/v PEG 20K). Well
328 diffracting crystals were grown via hanging-drop vapor diffusion in 0.1 M Tris, pH 8.0, 0.1 M NaCl, 5% w/v
329 PEG 20K and were frozen with 40% PEG 200 as a cryoprotectant. Diffraction data was collected at
330 Advanced Light Source beamline 5.0.3 at 12.7 keV. The dataset was processed using XDS [37] and AIMLESS
331 [38] to a resolution of 2.30 Å. Initial phases were solved by molecular replacement using Phaser in Phenix
332 [34] with a search model of ZikV sE protomer from PDBid 5JHM [39] and the AlphaFold3 [31] model of
333 F25.S02 Fab split into Fv and CH1/CL domains. Model building was completed using Coot [33] and

refinement was performed in Phenix. Additional model refinement was done using ISOLDE [35] in ChimeraX [32]. Data collection and refinement statistics are summarized in **Supplementary Table 2**. BSA data was determined using the PDBePISA server [36].

358

359 **References**


360 1. Bhatt S, Gething PW, Brady OJ, Messina JP, Farlow AW, Moyes CL, et al. The global distribution
361 and burden of dengue. Nature. 2013;496(7446):504-7. Epub 20130407. doi: 10.1038/nature12060.
362 PubMed PMID: 23563266; PubMed Central PMCID: PMCPMC3651993.
363 2. Weaver SC, Costa F, Garcia-Blanco MA, Ko AI, Ribeiro GS, Saade G, et al. Zika virus: History,
364 emergence, biology, and prospects for control. Antiviral Res. 2016;130:69-80. Epub 20160318. doi:
365 10.1016/j.antiviral.2016.03.010. PubMed PMID: 26996139; PubMed Central PMCID: PMCPMC4851879.
366 3. Kraemer MUG, Reiner RC, Jr., Brady OJ, Messina JP, Gilbert M, Pigott DM, et al. Past and future
367 spread of the arbovirus vectors Aedes aegypti and Aedes albopictus. Nat Microbiol. 2019;4(5):854-63.
368 Epub 20190304. doi: 10.1038/s41564-019-0376-y. PubMed PMID: 30833735; PubMed Central PMCID:
369 PMCPMC6522366.
370 4. Iwamura T, Guzman-Holst A, Murray KA. Accelerating invasion potential of disease vector Aedes
371 aegypti under climate change. Nat Commun. 2020;11(1):2130. Epub 20200501. doi: 10.1038/s41467-
372 020-16010-4. PubMed PMID: 32358588; PubMed Central PMCID: PMCPMC7195482.
373 5. Kuhn RJ, Zhang W, Rossmann MG, Pletnev SV, Corver J, Lenches E, et al. Structure of dengue
374 virus: implications for flavivirus organization, maturation, and fusion. Cell. 2002;108(5):717-25. doi:
375 10.1016/s0092-8674(02)00660-8. PubMed PMID: 11893341; PubMed Central PMCID:
376 PMCPMC4152842.
377 6. Rey FA, Heinz FX, Mandl C, Kunz C, Harrison SC. The envelope glycoprotein from tick-borne
378 encephalitis virus at 2 A resolution. Nature. 1995;375(6529):291-8. doi: 10.1038/375291a0. PubMed
379 PMID: 7753193.
380 7. Stettler K, Beltramello M, Espinosa DA, Graham V, Cassotta A, Bianchi S, et al. Specificity, cross-
381 reactivity, and function of antibodies elicited by Zika virus infection. Science. 2016;353(6301):823-6.
382 Epub 20160714. doi: 10.1126/science.aaf8505. PubMed PMID: 27417494.
383 8. Katzelnick LC, Gresh L, Halloran ME, Mercado JC, Kuan G, Gordon A, et al. Antibody-dependent
384 enhancement of severe dengue disease in humans. Science. 2017;358(6365):929-32. Epub 20171102.
385 doi: 10.1126/science.aan6836. PubMed PMID: 29097492; PubMed Central PMCID: PMCPMC5858873.
386 9. Katzelnick LC, Narvaez C, Arguello S, Lopez Mercado B, Collado D, Ampie O, et al. Zika virus
387 infection enhances future risk of severe dengue disease. Science. 2020;369(6507):1123-8. doi:
388 10.1126/science.abb6143. PubMed PMID: 32855339; PubMed Central PMCID: PMCPMC8274975.
389 10. Dengue vaccine: WHO position paper, September 2018 - Recommendations. Vaccine.
390 2019;37(35):4848-9. Epub 20181110. doi: 10.1016/j.vaccine.2018.09.063. PubMed PMID: 30424888.
391 11. Larson HJ, Hartigan-Go K, de Figueiredo A. Vaccine confidence plummets in the Philippines
392 following dengue vaccine scare: why it matters to pandemic preparedness. Hum Vaccin Immunother.
393 2019;15(3):625-7. Epub 20181012. doi: 10.1080/21645515.2018.1522468. PubMed PMID: 30309284;
394 PubMed Central PMCID: PMCPMC6605722.
395 12. Dejnirattisai W, Wongwiwat W, Supasa S, Zhang X, Dai X, Rouvinski A, et al. A new class of highly
396 potent, broadly neutralizing antibodies isolated from viremic patients infected with dengue virus. Nat
397 Immunol. 2015;16(2):170-7. Epub 20141215. doi: 10.1038/ni.3058. PubMed PMID: 25501631; PubMed
398 Central PMCID: PMCPMC4445969.
399 13. Rouvinski A, Guardado-Calvo P, Barba-Spaeth G, Duquerroy S, Vaney MC, Kikuti CM, et al.
400 Recognition determinants of broadly neutralizing human antibodies against dengue viruses. Nature.
401 2015;520(7545):109-13. Epub 20150112. doi: 10.1038/nature14130. PubMed PMID: 25581790.

402 14. Barba-Spaeth G, Dejnirattisai W, Rouvinski A, Vaney MC, Medits I, Sharma A, et al. Structural
403 basis of potent Zika-dengue virus antibody cross-neutralization. Nature. 2016;536(7614):48-53. Epub
404 20160623. doi: 10.1038/nature18938. PubMed PMID: 27338953.
405 15. Kam YW, Lee CY, Teo TH, Howland SW, Amrun SN, Lum FM, et al. Cross-reactive dengue human
406 monoclonal antibody prevents severe pathologies and death from Zika virus infections. JCI Insight.
407 2017;2(8). Epub 20170420. doi: 10.1172/jci.insight.92428. PubMed PMID: 28422757; PubMed Central
408 PMCID: PMCPMC5396524.
409 16. Zhang S, Loy T, Ng TS, Lim XN, Chew SV, Tan TY, et al. A Human Antibody Neutralizes Different
410 Flaviviruses by Using Different Mechanisms. Cell Rep. 2020;31(4):107584. doi:
411 10.1016/j.celrep.2020.107584. PubMed PMID: 32348755.
412 17. Lubow J, Levoir LM, Ralph DK, Belmont L, Contreras M, Cartwright-Acar CH, et al. Single B cell
413 transcriptomics identifies multiple isotypes of broadly neutralizing antibodies against flaviviruses. PLOS
414 Pathogens. 2023;19(10):e1011722. doi: 10.1371/journal.ppat.1011722.
415 18. FDA Approves First Respiratory Syncytial Virus (RSV) Vaccine [Internet]. U.S. Food and Drug
416 Administration; 2023. Available from: https://www.fda.gov/news-events/press-announcements/fda-
417 approves-first-respiratory-syncytial-virus-rsv-vaccine
418 19. Phan TTN, Hvasta MG, Kudlacek ST, Thiono DJ, Tripathy A, Nicely NI, et al. A conserved set of
419 mutations for stabilizing soluble envelope protein dimers from dengue and Zika viruses to advance the
420 development of subunit vaccines. J Biol Chem. 2022;298(7):102079. Epub 20220526. doi:
421 10.1016/j.jbc.2022.102079. PubMed PMID: 35643320; PubMed Central PMCID: PMCPMC9249817.
422 20. Sharma A, Zhang X, Dejnirattisai W, Dai X, Gong D, Wongwiwat W, et al. The epitope
423 arrangement on flavivirus particles contributes to Mab C10's extraordinary neutralization breadth across
424 Zika and dengue viruses. Cell. 2021;184(25):6052-66 e18. Epub 20211130. doi:
425 10.1016/j.cell.2021.11.010. PubMed PMID: 34852239; PubMed Central PMCID: PMCPMC8724787.
426 21. Yariv B, Yariv E, Kessel A, Masrati G, Chorin AB, Martz E, et al. Using evolutionary data to make
427 sense of macromolecules with a "face-lifted" ConSurf. Protein Sci. 2023;32(3):e4582. doi:
428 10.1002/pro.4582. PubMed PMID: 36718848; PubMed Central PMCID: PMCPMC9942591.
429 22. Contreras M, Stuart JB, Levoir LM, Belmont L, Goo L. Defining the impact of flavivirus envelope
430 protein glycosylation site mutations on sensitivity to broadly neutralizing antibodies. mBio.
431 2024;15(2):e0304823. Epub 20240109. doi: 10.1128/mbio.03048-23. PubMed PMID: 38193697;
432 PubMed Central PMCID: PMCPMC10865826.
433 23. Zhou T, Georgiev I, Wu X, Yang ZY, Dai K, Finzi A, et al. Structural basis for broad and potent
434 neutralization of HIV-1 by antibody VRC01. Science. 2010;329(5993):811-7. Epub 20100708. doi:
435 10.1126/science.1192819. PubMed PMID: 20616231; PubMed Central PMCID: PMCPMC2981354.
436 24. Parks KR, MacCamy AJ, Trichka J, Gray M, Weidle C, Borst AJ, et al. Overcoming Steric
437 Restrictions of VRC01 HIV-1 Neutralizing Antibodies through Immunization. Cell Rep. 2019;29(10):3060-
438 72 e7. doi: 10.1016/j.celrep.2019.10.071. PubMed PMID: 31801073; PubMed Central PMCID:
439 PMCPMC6936959.
440 25. Umotoy J, Bagaya BS, Joyce C, Schiffner T, Menis S, Saye-Francisco KL, et al. Rapid and Focused
441 Maturation of a VRC01-Class HIV Broadly Neutralizing Antibody Lineage Involves Both Binding and
442 Accommodation of the N276-Glycan. Immunity. 2019;51(1):141-54 e6. doi:
443 10.1016/j.immuni.2019.06.004. PubMed PMID: 31315032; PubMed Central PMCID: PMCPMC6642152.
444 26. Sevvana M, Long F, Miller AS, Klose T, Buda G, Sun L, et al. Refinement and Analysis of the
445 Mature Zika Virus Cryo-EM Structure at 3.1 A Resolution. Structure. 2018;26(9):1169-77 e3. Epub
446 20180626. doi: 10.1016/j.str.2018.05.006. PubMed PMID: 29958768; PubMed Central PMCID:
447 PMCPMC6125166.

448 27. Mastronarde DN. Automated electron microscope tomography using robust prediction of
449 specimen movements. J Struct Biol. 2005;152(1):36-51. doi: 10.1016/j.jsb.2005.07.007. PubMed PMID:
450 16182563.
451 28. Tegunov D, Cramer P. Real-time cryo-electron microscopy data preprocessing with Warp. Nat
452 Methods. 2019;16(11):1146-52. Epub 20191007. doi: 10.1038/s41592-019-0580-y. PubMed PMID:
453 31591575; PubMed Central PMCID: PMCPMC6858868.
454 29. Punjani A, Rubinstein JL, Fleet DJ, Brubaker MA. cryoSPARC: algorithms for rapid unsupervised
455 cryo-EM structure determination. Nat Methods. 2017;14(3):290-6. Epub 20170206. doi:
456 10.1038/nmeth.4169. PubMed PMID: 28165473.
457 30. Punjani A, Zhang H, Fleet DJ. Non-uniform refinement: adaptive regularization improves single-
458 particle cryo-EM reconstruction. Nat Methods. 2020;17(12):1214-21. Epub 20201130. doi:
459 10.1038/s41592-020-00990-8. PubMed PMID: 33257830.
460 31. Abramson J, Adler J, Dunger J, Evans R, Green T, Pritzel A, et al. Accurate structure prediction of
461 biomolecular interactions with AlphaFold 3. Nature. 2024;630(8016):493-500. Epub 20240508. doi:
462 10.1038/s41586-024-07487-w. PubMed PMID: 38718835; PubMed Central PMCID: PMCPMC11168924.
463 32. Meng EC, Goddard TD, Pettersen EF, Couch GS, Pearson ZJ, Morris JH, et al. UCSF ChimeraX:
464 Tools for structure building and analysis. Protein Sci. 2023;32(11):e4792. doi: 10.1002/pro.4792.
465 PubMed PMID: 37774136; PubMed Central PMCID: PMCPMC10588335.
466 33. Emsley P, Lohkamp B, Scott WG, Cowtan K. Features and development of Coot. Acta Crystallogr
467 D Biol Crystallogr. 2010;66(Pt 4):486-501. Epub 20100324. doi: 10.1107/S0907444910007493. PubMed
468 PMID: 20383002; PubMed Central PMCID: PMCPMC2852313.
469 34. Liebschner D, Afonine PV, Baker ML, Bunkoczi G, Chen VB, Croll TI, et al. Macromolecular
470 structure determination using X-rays, neutrons and electrons: recent developments in Phenix. Acta
471 Crystallogr D Struct Biol. 2019;75(Pt 10):861-77. Epub 20191002. doi: 10.1107/S2059798319011471.
472 PubMed PMID: 31588918; PubMed Central PMCID: PMCPMC6778852.
473 35. Croll TI. ISOLDE: a physically realistic environment for model building into low-resolution
474 electron-density maps. Acta Crystallogr D Struct Biol. 2018;74(Pt 6):519-30. Epub 20180411. doi:
475 10.1107/S2059798318002425. PubMed PMID: 29872003; PubMed Central PMCID: PMCPMC6096486.
476 36. Krissinel E, Henrick K. Inference of macromolecular assemblies from crystalline state. J Mol Biol.
477 2007;372(3):774-97. Epub 20070513. doi: 10.1016/j.jmb.2007.05.022. PubMed PMID: 17681537.
478 37. Kabsch W. Xds. Acta Crystallogr D Biol Crystallogr. 2010;66(Pt 2):125-32. Epub 20100122. doi:
479 10.1107/S0907444909047337. PubMed PMID: 20124692; PubMed Central PMCID: PMCPMC2815665.
480 38. Agirre J, Atanasova M, Bagdonas H, Ballard CB, Basle A, Beilsten-Edmands J, et al. The CCP4
481 suite: integrative software for macromolecular crystallography. Acta Crystallogr D Struct Biol. 2023;79(Pt
482 6):449-61. Epub 20230530. doi: 10.1107/S2059798323003595. PubMed PMID: 37259835; PubMed
483 Central PMCID: PMCPMC10233625.
484 39. Dai L, Song J, Lu X, Deng YQ, Musyoki AM, Cheng H, et al. Structures of the Zika Virus Envelope
485 Protein and Its Complex with a Flavivirus Broadly Protective Antibody. Cell Host Microbe.
486 2016;19(5):696-704. Epub 20160502. doi: 10.1016/j.chom.2016.04.013. PubMed PMID: 27158114.

487

488

489

490

491

492

493 **Acknowledgements**

494 We thank Dr. Brian Kuhlman for providing DenV3 and ZikV sE plasmids. We thank the J. B. Pendleton
495 Charitable Trust for its generous support of Formulatrix robotic instruments. This work was supported by
496 a Fred Hutch Vaccine and Infectious Disease Division (VIDD) Initiative grant. Electron microscopy data
497 were generated using the Fred Hutchinson Cancer Center Electron Microscopy Shared Resource. The
498 EMSR is supported in part by the Cancer Center Support Grant P30 CA015704. The Berkeley Center for
499 Structural Biology is supported in part by the Howard Hughes Medical Institute. The Advanced Light
500 Source is a Department of Energy Office of Science User Facility under Contract No. DE-AC02-05CH11231.
501 The ALS-ENABLE beamlines are supported in part by the National Institutes of Health, National Institute
502 of General Medical Sciences, grant P30 GM124169. A portion of this research was supported by the NIH
503 S10 instrumentation grant 1S10OD028581-01.

504

505 **Contributions**

506 N.K.H., J.L., L.G., and M.P. conceived the project. N.K.H., J.L., L.G., and M.P. designed the experiments.
507 N.K.H performed the cloning, expressed and purified the proteins, formed the complexes, collected and
508 processed the cryoEM data, and built and refined the model. N.K.H. crystallized the protein, collected and
509 processed the diffraction data, and solved the crystal structure. N.K.H., J.L., L.G., and M.P. analyzed and
510 discussed data. N.K.H. and M.P. wrote the original manuscript draft. N.K.H., J.L., L.G., and M.P. reviewed
511 and edited the manuscript. N.K.H., J.L., L.G. and M.P. secured funding for the project.

512

513 **Competing Interests**

514 J.L. and L.G. are inventors on a patent application filed by Fred Hutchinson Cancer Center relating to

515 F25.S02. The other authors have no competing interests.

516

517

518 **Figures**

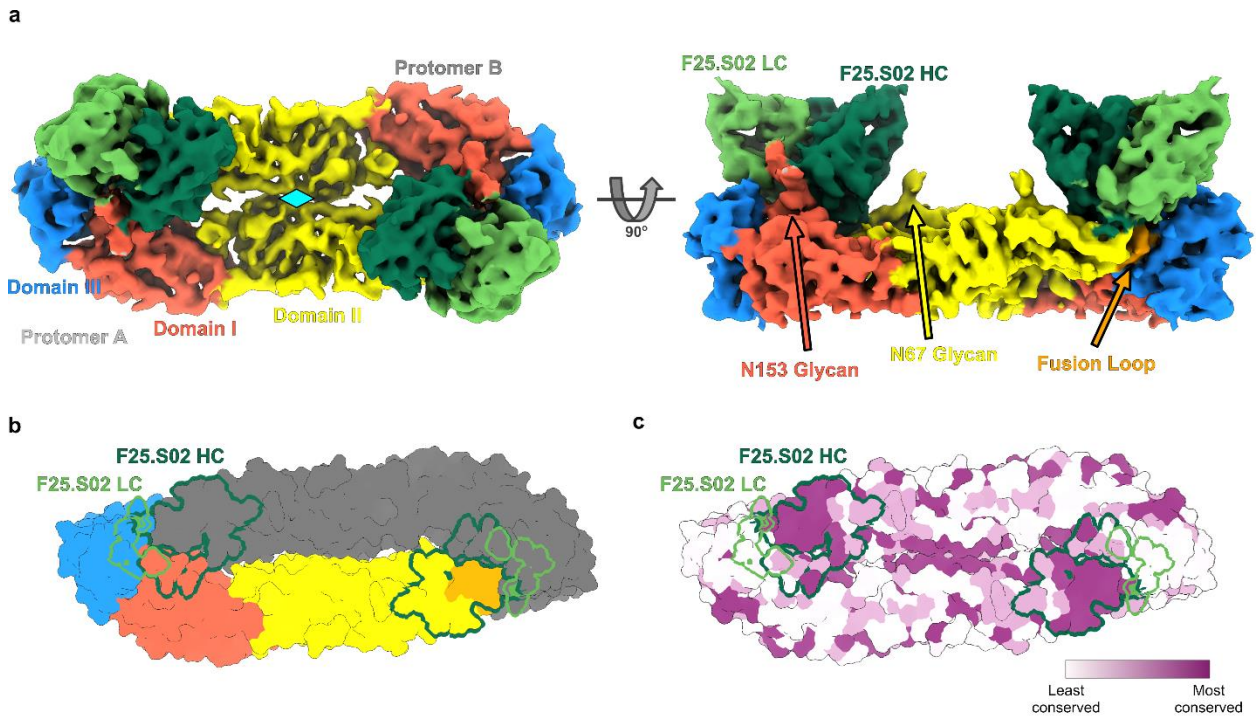


519

520 **Figure 1. CryoEM structure of F25.S02 bound to DenV3 sE** a) The cryoEM map of F25.S02 Fab bound to

521 DenV3 sE sc30. The map is colored to highlight the domains of the sE protein with the glycans labeled and

522 their locations shown. F25.S02 Fv is shown in dark green for the heavy chain and light green for the light

523 chain. Cyan diamond represents the 2-fold symmetry axis of the dimer. b) Model of DenV3 sE sc30 dimer

524 shown in surface representation with one protomer colored to show the domains and the other in gray.

525 The binding footprint of F25.S02 is highlighted with the heavy chain binding site in dark green and the

526 light chain in light green. c) The same model from b) but colored to show conservation of residues across

527 DenV serotypes and ZikV sE proteins. Coloring was generated using the ConSurf server.

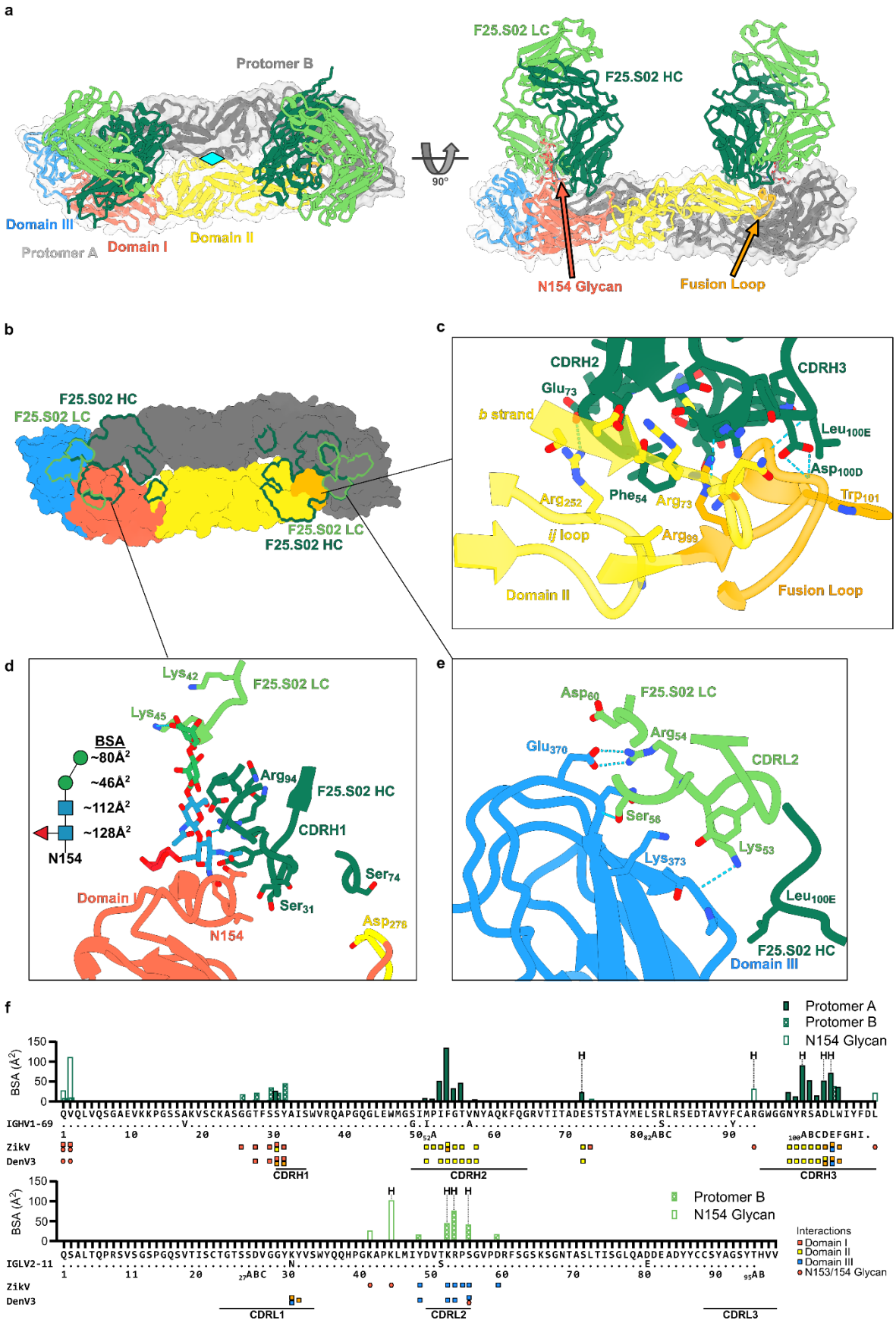
a
Protomer B
Domain III
Protomer A
Domain I
Domain II
F25.S02 LC
F25.S02 HC
90°
N154 Glycan
Fusion Loop
b
F25.S02 HC
F25.S02 LC
F25.S02 LC
F25.S02 HC
c
CDRH2
CDRH3
Glu73
b strand
Leu100E
Asp100D
Trp101
Arg252
Phe54
Arg73
jj loop
Arg99
Domain II
Fusion Loop
d
Lys42
F25.S02 LC
Lys45
BSA
~80Å2
~46Å2
~112Å2
~128Å2
N154
Arg94
F25.S02 HC
CDRH1
Ser74
Domain
Ser31
N154
Asp278
e
Asp60
F25.S02 LC
Arg54
Glu370
CDRL2
Ser56
Lys53
Lys373
Leu100E
F25.S02 HC
Domain III
f
Protomer A
Protomer B
N154 Glycan
BSA (Å2)
IGHV1-69
ZikV
DenV3
CDRH1
CDRH2
CDRH3
Protomer B
N154 Glycan
IGLV2-11
Interactions
Domain I
Domain II
Domain III
N153/154 Glycan
CDRL1
CDRL2
CDRL3

528

529 **Figure 2. X-ray crystal structure of F25.S02 bound to ZikV sE** a) The X-ray crystal structure of F25.S02 Fab
530 bound to ZikV sE dimer is shown in cartoon representation. The sE protein includes a transparent surface
531 representation with one protomer colored to highlight domains I, II, and III and the other shown in grey.
532 F25.S02 Fab is shown in dark green for the heavy chain and light green for the light chain. Cyan diamond
533 represents the 2-fold symmetry axis of the dimer. b) Surface representation of the ZikV sE dimer with the
534 F25.S02 epitope outlined in dark green for the heavy chain and light green for the light chain. c) Zoom in
535 of the binding interactions of F25.S02 with domain II and the fusion loop. Hydrogen bonds are indicated
536 by the blue dashed lines and interacting residues are labeled and shown in sticks. d) Zoom in of the binding
537 interactions of F25.S02 with domain I and the N154 glycan. Hydrogen bonds are indicated by the blue
538 dashed lines. The diagram of the N154 glycan is shown with the amount of BSA of each carbohydrate
539 listed. Blue square represents N-acetylglucosamine, red triangle is fucose, and green circle is mannose. e)
540 Zoom in of the binding interactions of F25.S02 with domain III. Hydrogen bonds are indicated by the blue
541 dashed lines. f) BSA plot showing which residues of F25.S02 are involved in the binding to ZikV sE. The
542 germline V-genes of both heavy and light chains are shown and the CDRs are indicated. The residues
543 involved in binding to ZikV and DenV3 sE are shown and color coded to indicate which domain they
544 interact with.

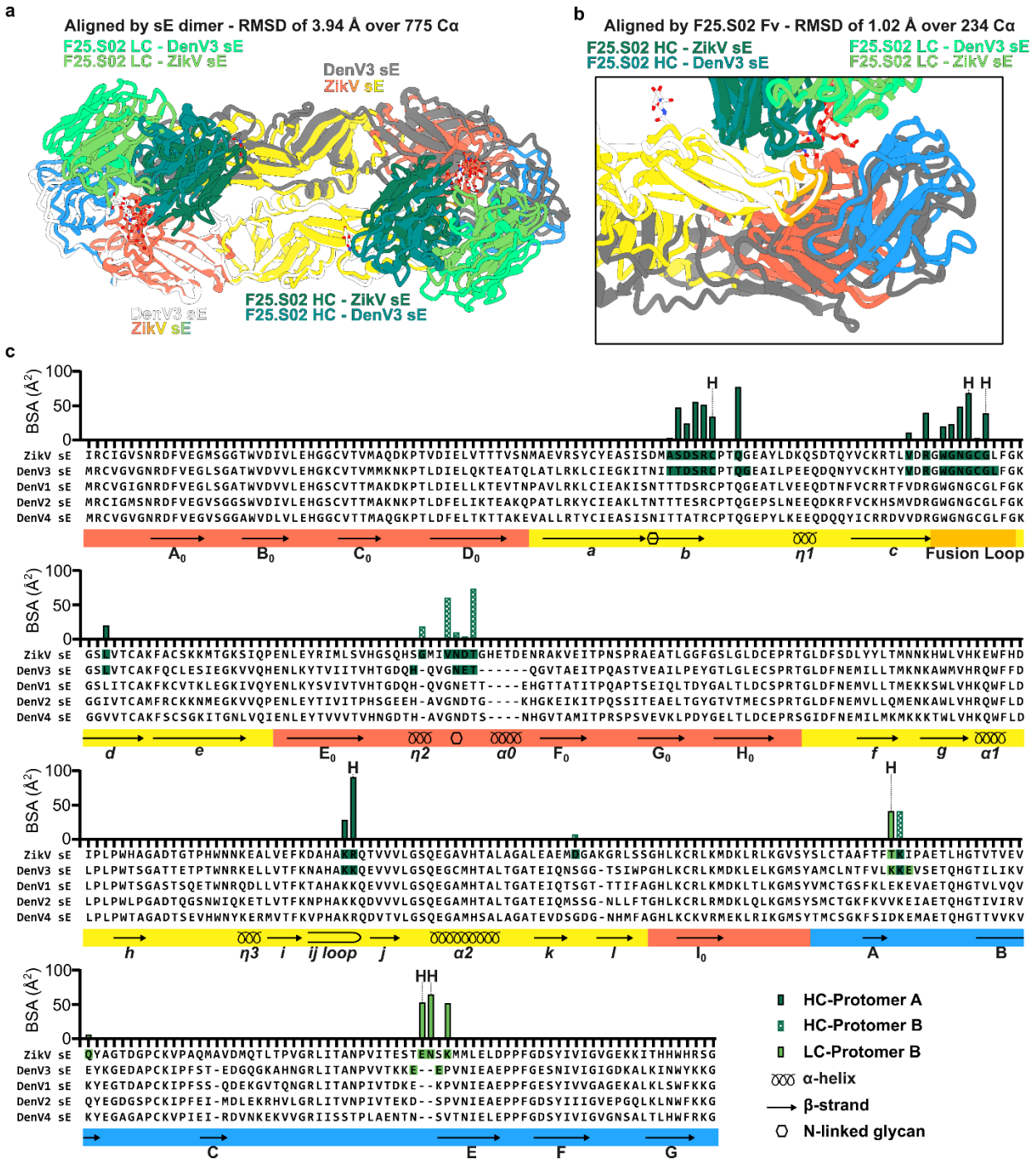


**Figure 3. Comparison of F25.S02 bound to DenV3 and ZikV sE** a) Alignment of ZikV and DenV3 sE structure. Alignment was made by matchmaking the sE dimer in ChimeraX. b) Alignment of ZikV and DenV3 sE structure highlighting a single Fab-dimer interaction. Alignment was made by matchmaking the Fv domain of F25.S02 in ChimeraX. c) BSA plot of ZikV sE bound by F25.S02 with an alignment of DenV1-4

550 sE. The DenV3 residues interacting with F25.S02 are highlighted in the alignment. The domains and fusion

551 loop are colored and the secondary structural elements of ZikV sE as well as the N-linked glycan sites are

552 shown.

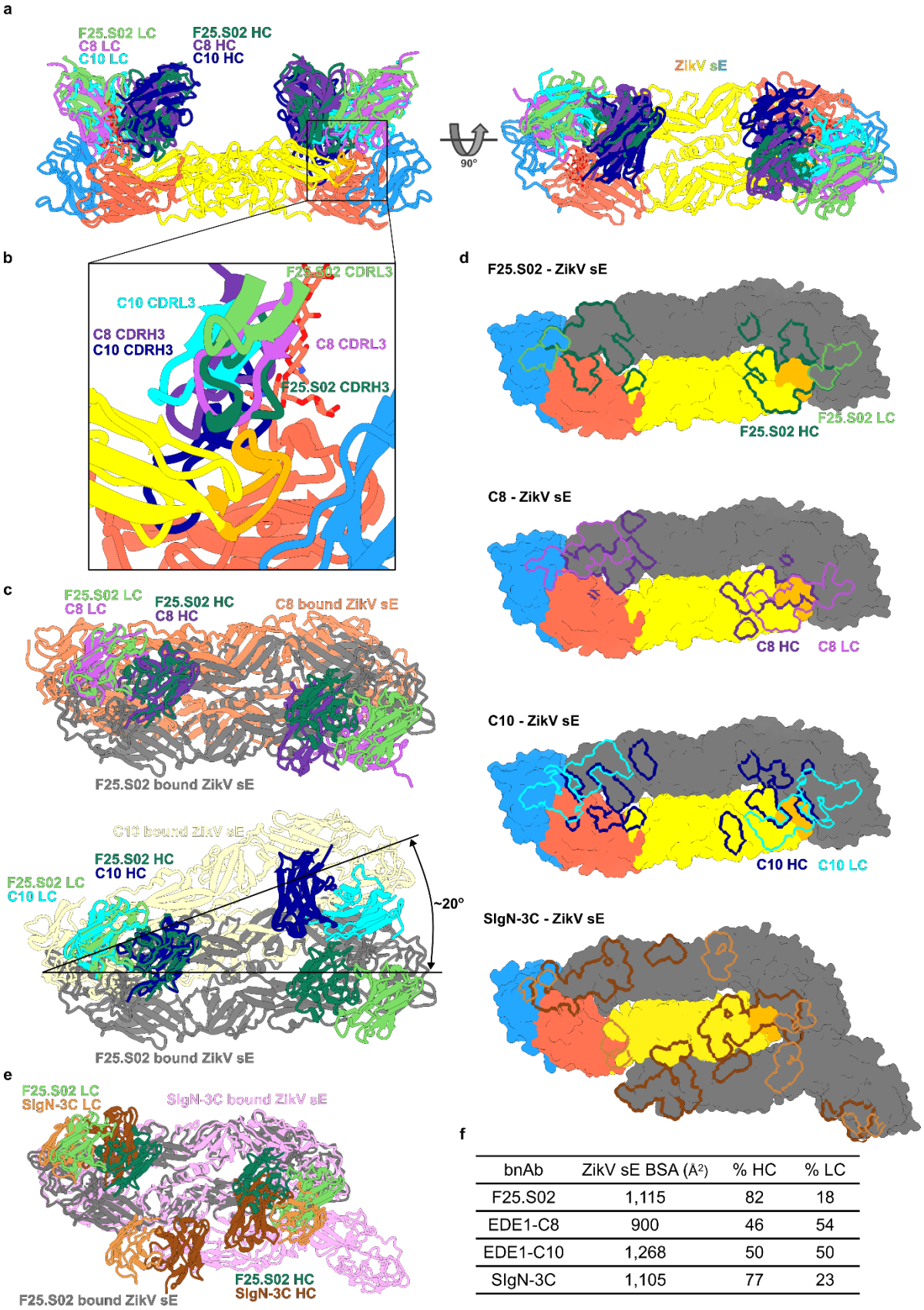


f

| bnAb | ZikV sE BSA (Å²) | % HC | % LC |
|---|---|---|---|
| F25.S02 | 1,115 | 82 | 18 |
| EDE1-C8 | 900 | 46 | 54 |
| EDE1-C10 | 1,268 | 50 | 50 |
| SIgN-3C | 1,105 | 77 | 23 |

553

554 **Figure 4. Structural comparison of F25.S02 to other orthoflavivirus bnAb** a) Alignment of EDE1
555 antibodies, C8 and C10, bound to ZikV sE and the F25.S02 bound ZikV sE. Alignment was made by
556 matchmaking the sE dimer in ChimeraX. Only the F25.S02 bound ZikV sE is shown for simplicity. b) Zoom
557 in of the interactions of F25.S02, C8, and C10 to the fusion loop. Both C8 and C10 CDRL3 bind in the
558 location of the F25.S02 CDRH3. c) Alignment of C8 and C10 to F25.S02 by Fv domain of one Fab in the
559 dimer. Alignment of C8-ZikV sE and F25.S02-ZikV sE (top). Alignment of C10-ZikV sE and F25.S02-ZikV sE
560 (bottom). d) Surface representation of the ZikV sE dimer with epitopes of F25.S02, C8, and C10 outlined.
561 e) Alignment of F25.S02 and SIgN-3C of bound ZikV sE dimer. The alignment was made by matchmaking
562 the sE dimer in ChimeraX. F) Table showing the total BSA of each bnAb footprint on ZikV sE and the
563 respective contribution of the heavy and light chains.

564

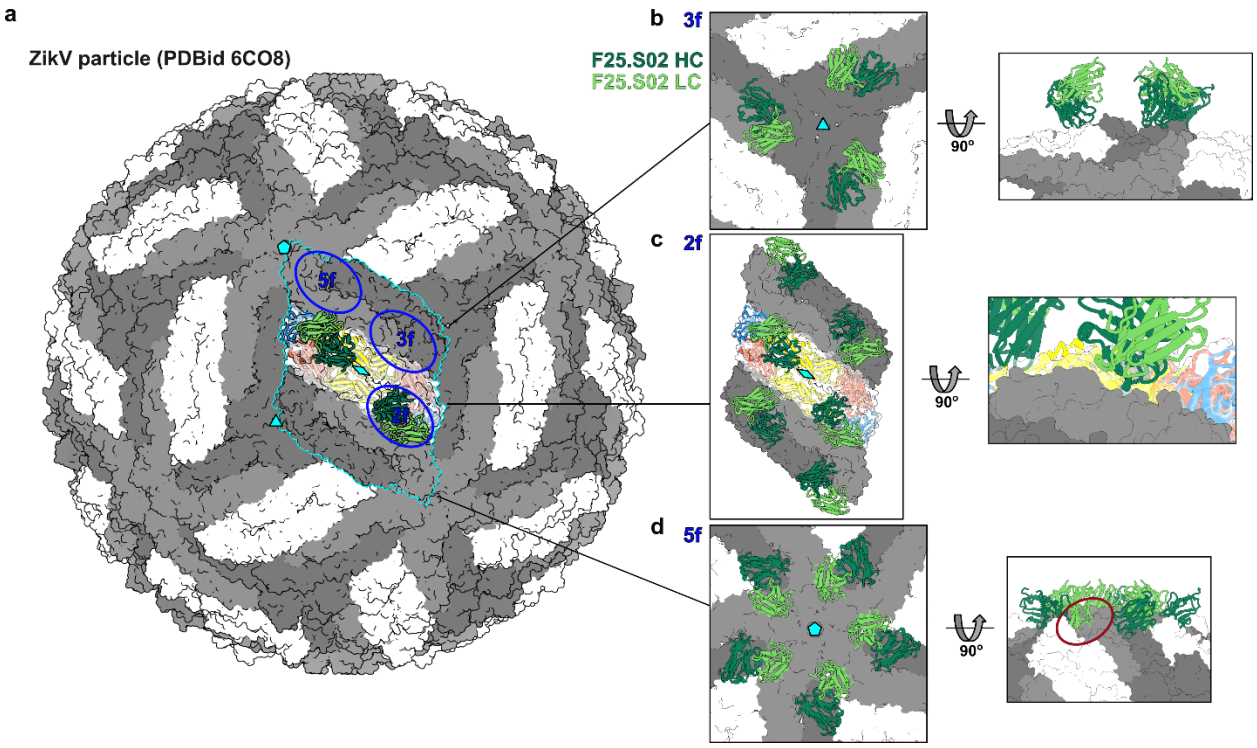


565

566

567 **Figure 5. Alignment of F25.S02 to ZikV viral particle** a) Alignment of the F25.S02-ZikV sE crystal

568 structure on the whole virus cryoEM structure of ZikV (PDBid 6CO8). The sE raft is highlighted in cyan.

569 The sE dimer 2-fold symmetry is shown by the diamond, the icosahedral 3-fold and 5-fold symmetry

570 axes are shown by the triangle and pentagon, respectively. The E protein binding sites, 2f, 3f, and 5f are

571 shown with blue circles b) Zoom in showing potential binding of F25.S02 at the 3f site. c) zoom in

572 showing potential F25.S02 binding in an E protein raft on the particle. d) Zoom in showing potential

573 binding of F25.S02 at the 5f site. Light chain would potentially clash with adjacent dimer.

574

575